

Mechanism of Aortic Injury in Nearside Left Lateral Automotive Crashes: A Finite Element Accident Injury Reconstruction Approach

Aditya Belwadi, King H. Yang
Wayne State University, Detroit, MI

Abstract Traumatic rupture of the aorta (TRA) remains the second most common cause of death associated with motor vehicle crashes (MVC), only less prevalent than brain injury. On an average, nearly 8,000 people die annually in the United States due to blunt injury to the aorta. It is observed that over 80% of occupants who suffer an aortic injury die at the scene due to exsanguination into the chest cavity. There have been numerous hypotheses for aortic injury in the literature but it is imperative to draw a distinction between the injury mechanisms in different directions of impact.

Eight real world crashes were reconstructed in two stages using a combination of accident investigation data from the Crash Injury Research and Engineering Network (CIREN) database, finite element (FE) vehicle models, and Wayne State Human Body Model (WSHBM). Further, 16 design of computer experiments (DOCE) simulations were carried out to understand the effect of key factors (Principle Direction of Force (PDOF), impact position, impact angle, velocity of impact, and the bumper profile of striking vehicle) on average maximum principal strain (AMPS) and maximum pressure in the aorta. In order to get a better understanding of the mechanism of TRA, a sensitivity study was performed using a combination of WSHBM and a variation of PDOF. The AMPS and maximum pressure due to longitudinal stretch of the thoracic aorta was the highest at a PDOF of 270 degrees of impact and the occupant seated adjacent to the B-pillar. As the PDOF increased from 250 degrees to 310 degrees, the aortic arch transitioned from a caudomedial motion of the thoracic spine relative to the sternum (owing to thoracic deformation from the intruding B-pillar) to posterior-anterior motion of the thoracic aorta relative to the ascending aorta due to thoracic compression (greater than 300-degree impact).

Keywords Accident reconstruction, aortic injury, injury biomechanics, principle direction of force, side impact

I. INTRODUCTION

Traumatic Rupture of the Aorta (TRA) remains the leading cause of death after head trauma. Over the last four decades, closed chest trauma concerning ruptures of the thoracic organs and blood vessels have caused 25-40% of all automotive fatalities in which 10-20% of those fatalities were due to aortic trauma [34]. In side impacts (left and right inclusive), the incidence is higher at 2.4% than those in frontal impacts at 1.1% [29][30]. In spite of advances in the surgical techniques using endovascular prostheses, more than 60% of motor vehicle crash (MVC) induced TRAs die at the scene and another 20% die during transportation and during surgical intervention [30]. Hence, it is imperative to have a better understanding of the mechanism of injury to aid development of suitable prevention techniques.

There have been numerous hypotheses made on injury mechanisms for TRA, based on: *inertia* ([6], [11], [15], [22]); *pressure* ([4], [13], [16], [19], [20], [23], [29], [32]); *strain* ([9], [10], [21], [27], [28]); *atherosclerosis* ([8], [16], [31], [33]); and *other factors* ([2], [3], [5], [12], [17], [18], [25], [35], [36]). Unfortunately, data published in the literature lack the usage of real world crash data and reconstruction methodology. Further, it is imperative to draw a distinction between the injury mechanisms in different directions of impact.

Aditya Belwadi is a Post-Doctoral fellow at the Center for Injury Research and Prevention, The Children's Hospital of Philadelphia. The current work was carried out as part of his doctoral dissertation in Biomedical Engineering from Wayne State University in Detroit, MI (Ph.: (313) 878-8601; Fax.: (313) 577-8333; Email: adityabn@gmail.com); King H. Yang is a Professor in the Biomedical Engineering department at Wayne State University in Detroit, MI

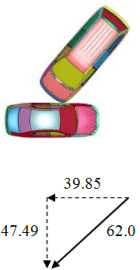
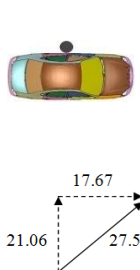
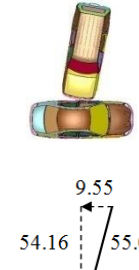
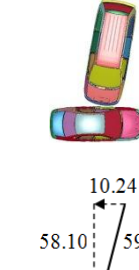
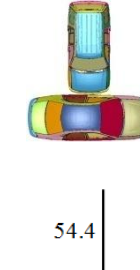
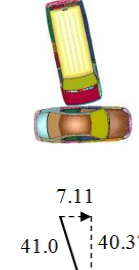
II. METHODS

Eight near side left lateral automotive crashes in which a TRA occurred were reconstructed in two stages using a combination of accident reports obtained from the Crash Injury Research and Engineering Network (CIREN) database, FE vehicle models, and Wayne State Human Body Model (WSHBM) [26]. The WSHBM represents a 50th percentile adult male model measuring 5' 10" in height and weighing 172 pounds. Four FE car models, a Ford Taurus, Ford Explorer, Dodge Caravan and a Ford Econoline 350, were taken from the National Crash Analysis Center (NCAC) FE model archive (<http://www.ncac.gwu.edu/vml/models.html>) and used as baseline models. In Stage I, the struck and the striking FE vehicle models were scaled to match with the overall dimensions such as the wheelbase, width, and height. The driver's weight (from the case data) was compensated for by adding a lumped mass to the center of gravity of the driver's seat. Similarly, the striking vehicle was scaled, the two vehicles were positioned, and initial velocity applied to the striking vehicle as a vector component defined by the PDOF calculated from accident investigation data. In Stage II, the interface files, which consist of nodal kinematic histories and the sub-model (left door structures) of the case vehicles' structures that might interact with the occupant, were used as inputs to the WSHBM. The occupant model was positioned in a seated posture estimated from post-crash photographs of interior structures and the seat position; contact interfaces were created and simulated using LS-DYNA. Table 1 details the relevant information obtained from the CIREN database while Table 2 lists important parameters needed for the accident reconstruction. As shown in Table 2, four basic FE car models were used to create all vehicle models involved in the crashes.

Table 1: Summary of nearside left lateral cases used in the accident injury reconstruction process

Parameter	Case 4	Case 5	Case 6	Case 7	Case 8	Case 15	Case 16	Case 17	
				Crash Details					
Impact Object	Car-Car	Car-Tree	Car-SUV	Car-Car	Car-Pole	Car-SUV	Car-SUV	Car-Van	
Delta V (km/hr)	62	27.5	55	59	27.6	47	54.4	41	
PDOF (Degree)	310	310	280	280	320	270	270	260	
Seat Belt Usage	Two-point shoulder belt, no lap belt	Three-point belt	Three-point belt, not in use	Three-point belt	Three-point belt	No belt	No belt	Three-point belt	
				Occupant Details					
Status	Survived	Fatal	Fatal	Fatal	Fatal	Fatal	Fatal	Survived	
Age (Years) (37±15)	29	24	28	34	65	35	27	55	
Race	Hispanic	Caucasian	African-American	African-American	Caucasian	Caucasian	African-American	Caucasian	
Gender	Male	Male	Male	Male	Male	Female	Male	Male	
Height (cm) (174.1±8.5)	183	171	185	163	181	175	172	163	
Weight (kg) (93.1±7.7)	100	91	84	83	101	99	87	100	
Aortic injury details	50% aortic transection of the intimal surface at the level of the aortic isthmus which was contained within the tissues of the posterior mediastinum	Complete transection of the thoracic aorta, 4 centimeters distal to the left subclavian artery at the level of the isthmus	Aortic transection 4 centimeters in length, 1.5 centimeters distal to left subclavian artery	Transverse laceration of the aortic isthmus, 3 centimeters in length on the posterior right side of the isthmus, located 3.5 centimeters distal to the left subclavian artery	Transverse laceration of the aortic isthmus, 4.5 centimeters in length just distal to the left subclavian artery orifice	Complete aortic transection at the level of the isthmus, 2 centimeters distal to the left subclavian artery orifice	A second laceration of the isthmus occurred, 2 centimeters below the left subclavian orifice	Aortic isthmus disruption which was contained within the posterior mediastinal tissues	

Table 2: Summary of vehicle models used in the left lateral Crash reconstruction process

Parameter	Case 4	Case 5	Case 6	Case 7	Case 8	Case 15	Case 16	Case 17
Case Vehicle (Year, Make and Model)	1992 Volkswagen Jetta sedan	2001 Honda Prelude coupe	2000 Mazda 626 sedan	1993 Toyota Corolla Sedan	1994 Honda Accord sedan	1985 Oldsmobile Cutlass Ciera sedan	1997 Mazda 626 sedan	2002 Dodge Stratus sedan
Case Vehicle Weight (kg)	1,046	1,467	1,299	1,085	1,469	1,257	1,320	1,432
FE Vehicle Model Used (Year, Make and Model)	2001 Ford Taurus sedan	2001 Ford Taurus sedan	2001 Ford Taurus sedan	2001 Ford Taurus sedan				
Striking Vehicle (Year, Make and Model)	1992 Volkswagen Jetta sedan	Tree	2000 Honda CRV SUV	1996 Dodge Caravan mini-van	Pole	1994 Nissan Pathfinder SUV	1998 Toyota RAV 4 SUV	1998 Ford Econoline 350 van
Striking Vehicle Weight or Fixed Object Diameter	1,046 kg	0.46 m	1,452 kg	1,612 kg	0.46 m	1,812 kg	1,356 kg	2,547 kg
FE Vehicle Model Used (Year, Make and Model)	2001 Ford Taurus sedan	Solid Elements	1998 Ford Explorer SUV	2002 Dodge Caravan mini-van	Solid Elements	1998 Ford Explorer SUV	1998 Ford Explorer SUV	1998 Ford Econoline 350 van
Initial Model Setup in the Simulation (km/hr)								

To further understand the effect of several crash factors which may affect the risk of aortic injury, a design of computer experiments study (DOCE) was performed on 16 runs generated using a Latin Square method in modeFRONTIER 4.0 (ESTECO North America). Five design factors were chosen, each with two to four levels of variation: impact height/bumper profile, impact position, PDOF, and initial velocity of the bullet vehicle along with varying occupant-seating positions in the case vehicle. Table 3 lists the design factors and ranges simulated, while Fig. 1(a) and Fig. 1(b) graphically demonstrate these locations.

Table 3: Range of values for the five design factors chosen for the DOCE study

No.	Design Factor	Range
1	Impact Height / Bumper Profile	Low High - -
2	Striking Vehicle Impact Position (mm)*	- 300 0 + 300 -
3		PDOF (degrees) 250 270 290 310
4	Initial velocity (km/hr)	30 38.3 46.6 54.9
5	Struck Vehicle Occupant Position (mm)*	-125 0 + 125 -

*Note: Impact Position and Occupant Position are determined from the center of the case vehicles' B-pillar

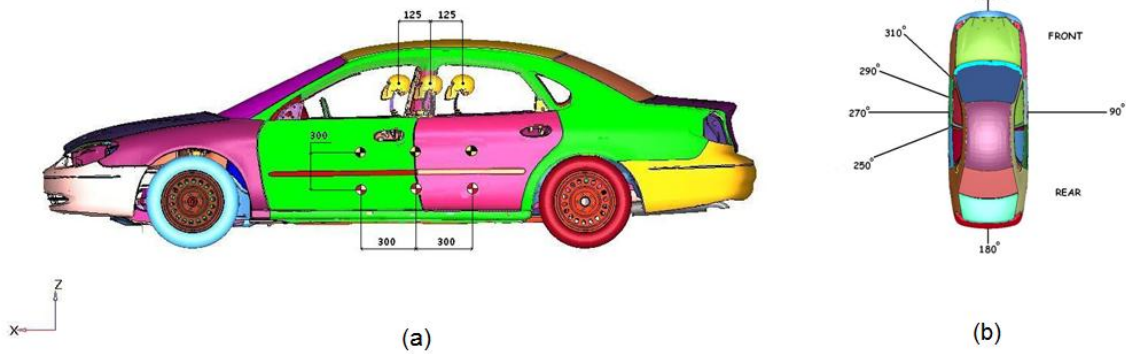


Fig. 1: (a) Position of the impact vehicle, height of impact and occupant seating position (b) Range of PDOF in the simulations

A 2001 FE Ford Taurus model, similar to the struck vehicle in the selected case, was used as the baseline target vehicle for the DOCE study. For the striking vehicle, FE models of a 2002 Dodge Caravan, which has a low bumper profile similar to a sedan, and a 2002 Ford Explorer, which has a higher bumper profile than a sedan, were used for the simulations. Impact positions were chosen to be the center, 300 mm forward or 300 mm backward of the case vehicles' B-pillar. The PDOF (from 250 to 310 degrees) and initial velocity (from 30 to 54.9 km/hr) were chosen to cover the range of values in previous CIREN cases. Finally, the occupant seating position selected covered the range of fore-aft range of the seat (250 mm) for a 2001 Ford Taurus with the angle of seat back at 110 degrees. That is, the occupant was positioned mid-track, 125 mm forward of mid-track or 125 mm backward of mid-track.

The response variables were the average maximum principal strain (AMPS) and maximum pressure in the aorta. For AMPS, four adjacent elements in the region with the highest maximum principal strains were selected and averaged; while for pressure, the maximum value in a single aortic element obtained during the entire simulation were tabulated. Binary logistic regression method was used to analyze failure versus non-failure modes in the reconstructed CIREN cases.

III. RESULTS

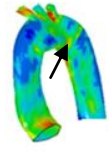
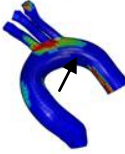
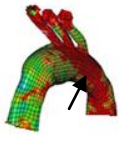
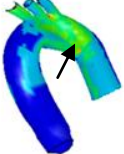
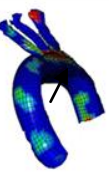
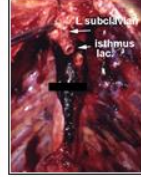
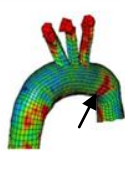
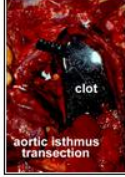
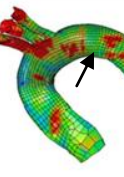
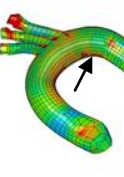
Table 4 lists the human model predicted maximum principal strain averaged from four elements in the isthmus region and the maximum pressure in the aorta for the eight CIREN cases simulated, while Table 5 compares the locations of high isthmus strains calculated by the FE model with the real world CIREN data.

Table 4: Output details for the FE reconstructions – Stage II

CIREN Case No.	PDOF (Deg)	Delta 'V' (km/hr)	Occupant Status	Left Side Door Structure Impact Time with Occupant (ms)	Average Maximum Principal Strain at the Isthmus (AMPS)*	Time at AMPS (ms)	Maximum Pressure (kPa)	Time at Maximum Pressure (ms)
4	310	62	Survived	14	0.1452	56	114.8	48
5	310	27.5	Fatal	34	0.1658	54	108.7	60
6	280	55	Fatal	16	0.2767	30	134.0	30
7	280	59	Fatal	22	0.2823	40	132.2	36
8	320	27.6	Fatal	30	0.1851	50	104.6	50
15	270	47	Fatal	26	0.1921	42	102.0	47
16	270	54.4	Fatal	22	0.2955	36	136.0	35
17	260	41	Survived	33	0.1941	42	103.8	52
Average					0.217±0.059		117.01±14.67	

*AMPS: Average maximum principal strain at the level of the isthmus calculated from four elements in the isthmus region.

Table 5: Comparison of injury locations between real world CIREN data and FE model predicted regions of strain

Case #4		Case #5		Case #6		Case #7	
CIREN data	Model Predicted	CIREN data	Model Predicted	CIREN data	Model Predicted	CIREN data	Model Predicted
							
Case #8		Case #15		Case #16		Case #17	
CIREN data	Model Predicted	CIREN data	Model Predicted	CIREN data	Model Predicted	CIREN data	Model Predicted
							

The maximum principal strains ranged from 14.5% to 29.6% and the pressures ranged from 102 kPa to 136 kPa for the eight CIREN cases simulated. For the two victims who sustained aortic injury but survived the crashes (Cases 4 and 17), the average AMPS was 17% and the average maximum pressure was 109 kPa. On the other hand, for the six cases with a fatal crash, the average AMPS was 23.3% and the average maximum pressure was 120 kPa. Table 6 lists the inputs for the DOCE simulation matrix and the response variables. Some simulations terminated earlier due to ‘negative volume’ based on LS-DYNA terminology.

Table 6: Latin Square sampling for the DOCE study along with output response variables: Average Maximum Principal Strain (AMPS) and maximum pressure in the aorta

Run #	Bumper Profile Height	Impact Position (mm)	PDOF (Degrees)	Velocity (km/hr)	Occupant Position (mm)	Maximum Simulation Time (ms)	AMPS*	Time at AMPS (ms)	Maximum Pressure (kPa)	Time at Maximum Pressure (ms)
1	Low	-300	290	30.0	+125	56	0.118	55	105.8	50
2	Low	-300	270	38.3	0	65	0.224	44	113.5	46
3	High	-300	250	46.6	-125	54	0.165	54	148.0	48
4	High	-300	310	54.9	0	33	0.054	33	109.0	33
5	Low	0	270	54.9	0	52	0.324	40	135.0	36
6	Low	0	290	46.6	+125	46	0.158	44	119.6	36
7	High	0	310	30.0	0	78	0.067	78	104.4	70
8	High	0	250	38.3	-125	64	0.165	56	120.0	50
9	Low	0	310	46.6	-125	80	0.210	60	127.6	50
10	Low	0	250	54.9	0	44	0.258	43	117.7	42
11	High	0	290	38.3	0	44	0.033	43	104.3	42
12	High	0	270	30.0	+125	70	0.152	54	110.8	54
13	Low	+300	250	38.3	0	72	0.230	44	113.2	48
14	Low	+300	310	30.0	-125	80	0.025	78	91.0	78
15	High	+300	270	54.9	+125	36	0.235	34	149.0	34
16	High	+300	290	46.6	0	76	0.160	54	123.7	52
Average							0.154±0.08		117.2±12.1	

* Average Maximum Principal Strain = Lower Surface Average Maximum Tensile Principal Strain in the longitudinal axis of the aorta

From the DOCE simulations, a maximum strain of 32.4% was recorded in Run #5 at a pressure of 135 kPa, which was a sedan impacting the B-pillar (270 degrees) at 55 km/hr with the occupant seated at the B-pillar. The lowest strain of 2.5% was observed in Run #14 at a pressure of 91.0 kPa, which was a sedan impacting 300 mm to the left of B-pillar at an angle of 310 degrees and a velocity of 30 km/hr with the occupant seated 125 mm in front of the B-pillar.

IV. DISCUSSION

Traumatic rupture of the aorta has been identified as the second most common cause of early death following MVC, only surpassed by brain injury [24]. Because of the high mortality rate of aortic injury, 59% deaths at the scene of the crash, and in some studies up to half of the scene survivors dying in transport or in the ER of the receiving hospital, considerable experimental efforts have been expended to define the causative factors that produce this injury [7].

From Stage I and Stage II simulation runs performed in this study, a trend in the location with the highest AMPS in the aorta was evident. All the reconstructions had high strains in the isthmus region, distal to the left subclavian artery with stretching of the three great vessels (Fig. 2a), and the injury source being the side door structures including the arm rest, door interior structures, and the B-pillar (Fig. 2b).

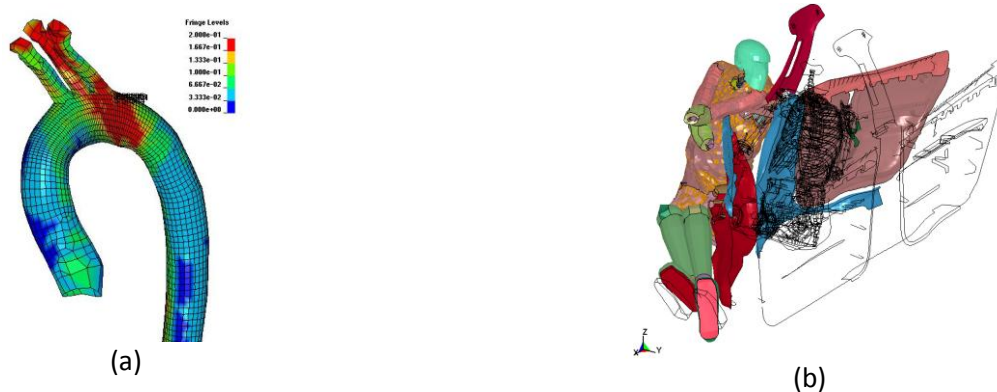


Fig. 2: (a) Average maximum principal strain location – isthmus of the aorta, (b) Left side door intrusion pattern

A logistic regression was performed on AMPS (Fig. 3a) and maximum pressure (Fig. 3b) for the eight CIREN cases reconstructed. A 50% risk of aortic failure was 16.5% strain based on AMPS and 97 kPa based on maximum pressure in the aorta. Alternatively, a 90% risk of failure for AMPS was 22% strain and 130 kPa for maximum pressure in the aorta. A Chi-Square Goodness-of-Fit Test revealed insignificant Pearson’s coefficient (5.472 for AMPS and 6.809 for maximum pressure).

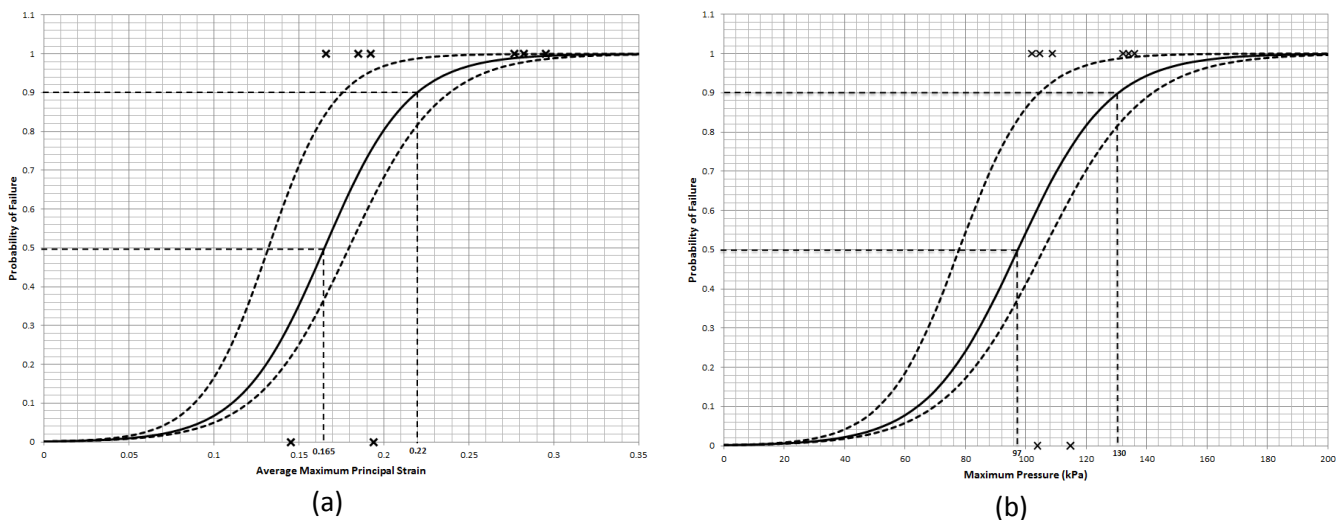


Fig. 3: Logistic Regression plot with 95th percentile confidence intervals for (a) AMPS (b) Maximum Pressure

Reference [1] reported a 50% risk of tear to the aorta at 101 kPa and increased it to 120 kPa for occupants 68 years of age based on aortic pressurization tests on 13 cadaveric aortas (10 *in vitro*, 3 *in situ*). Reference [10] tested eight unembalmed pressurized cadavers in an inverted configuration and subjected them to a battery of pendulum (32-kg impactor with a 152 mm face) impact tests. The average intraluminal pressure in the aorta ranged from 33.5 to 165.0 kPa with an average of 67.5 kPa. These experimentally obtained values are of the

same order of magnitude with the current study in which a 50% and 90% risk of aortic rupture was 97 and 130 kPa, respectively.

Reference [25] concluded from *in vitro* biaxial tensile tests at 1 m/s on cruciate shaped specimens that the average longitudinal failure strain to be 23.2% in the ascending region, 27.3% in the descending region and 25.1% in the peri-isthmus region, with an overall average failure strain of 24.4%. In a second series of longitudinal stretch tests conducted by [26] on whole aortas until failure (1 m/s), an average failure strain of 22.1% was reported. It should be noted that the strain data published in both series of tests were based on isolated aortic specimens and few specimens failed around the region of atherosclerotic plaque deposits. Reference [10] in their tests of eight unembalmed cadavers reported an average aortic failure strain of 0.208 ± 0.216 . In the current study, 22% AMPS represents a 90% risk of aortic rupture and seems to match these experimental data well. Obviously, the number of non-failure (non-fatal) cases (n=2) is insufficient for statistical analysis and the magnitude is only valid for the current numerical model.

In order to determine critical factors for the DOCE simulation, main effects analysis was performed in Minitab 16.1 (Minitab Inc., PA) based on the FE model predicted results listed in Table 6. Figures 4 and 5 summarize the relationships between selected design factors and AMPS in the isthmus (Fig. 4) or peak pressure in the aorta (Fig. 5) predicted by the WSHBM.

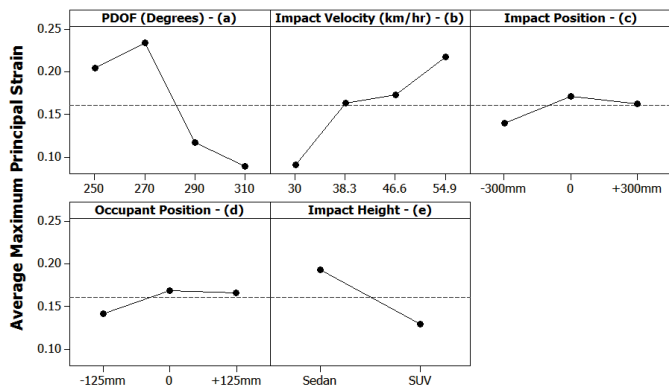


Fig. 4: Main effects chart for Average Maximum Principal Strain

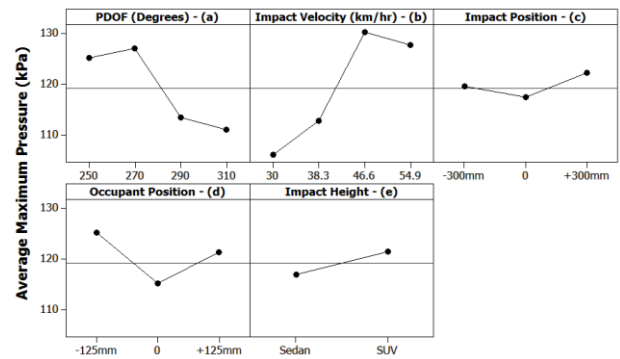


Fig. 5: Main effects chart for Maximum Pressure (kPa)

It is noted that a PDOF of 270 degrees resulted in the highest average AMPS (Fig. 4a) among all factors and levels studied. An increase in impact velocity had a direct correlation with the increase in AMPS (Fig. 4b), while an occupant seated adjacent to the B-pillar with an impact directed to the B-pillar seemed to generate higher strain in the isthmus region (Fig. 4c and Fig. 4d). Bumper height yielded results in contrast to intuitive thinking. Impacts from the lower profile Dodge caravan generated a higher isthmus strain compared to a higher profile SUV represented here by a Ford Explorer model (Fig. 4e). It was observed that, in runs with lower bumper profile, the armrest gets pushed into the thorax causing severe localized deformation, leading to increased AMPS and maximum pressure; which does not occur with a higher bumper profile. Further, because of the mass difference of 488.5 kilograms between the Dodge Caravan (2,028.1 kg) and the Ford Explorer (1,539.6 kg) FE models, the difference in momentum between the two impacts might have had an effect on the intrusion pattern. A one-way ANOVA performed between the two FE models for AMPS ($p=0.136$) and maximum pressure in the aorta ($p=0.58$) did not show statistical significance.

From Fig. 5a, a PDOF of 270 degrees resulted in the highest aortic pressure among all four PDOF's simulated. As the impact velocity increased, the aortic pressure also increased and seemed to vary negligibly after a velocity of 46.6 km/hr (Fig. 5b). In contrast to the findings for AMPS, an impact position centered on the B-pillar (Fig. 5c) or an occupant seated adjacent to the B-pillar (Fig. 5d) generated the lowest aortic pressures, and a higher bumper profile generated a higher aortic pressure (Fig. 5e).

The effects for coupled variables were analyzed using Pareto charts (Fig. 6). In a Pareto chart, the length of the bars indicates absolute value of each individual and coupled variable's effect. The Lenth method based on a t-distribution was specially designed to study the effect of computer experiments by assuming that only small shares of variables are significant [14]. From Fig. 6a, it is observed that a combination of PDOF and occupant

seating position followed by bumper profile height with occupant position have a significant impact on the AMPS while a combination of PDOF and occupant seating position followed by bumper profile height with occupant seating position had a significant impact on the maximum pressure generated in the aorta in the 16 simulations (Fig. 6b).

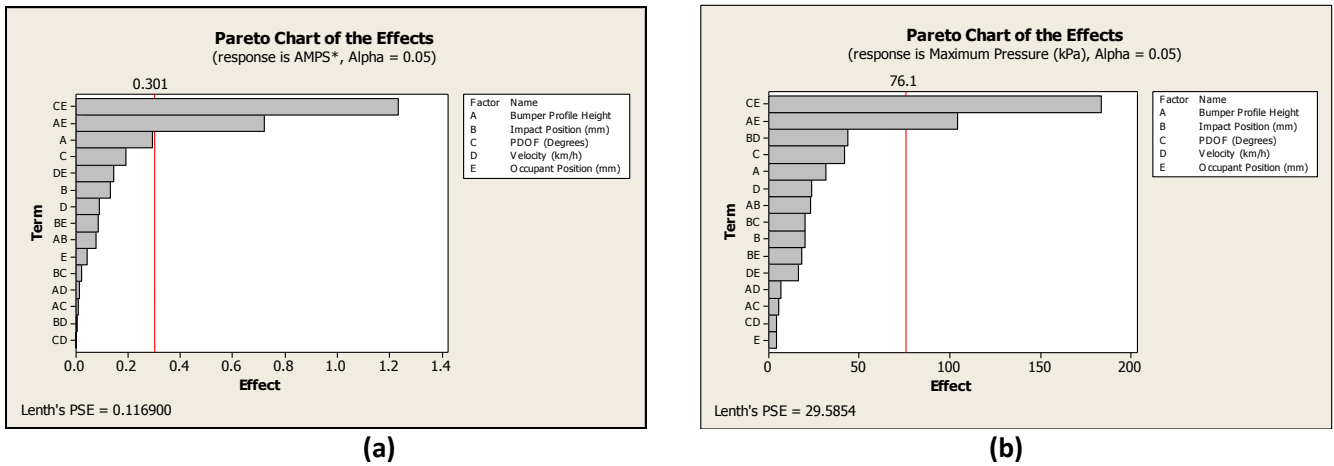


Fig. 6: Pareto chart of effects for combined factors (a) AMPS (b) Maximum Pressure

From the DOCE simulations, it was evident that PDOF and occupant seating position combined had a significant effect on AMPS and maximum pressure in the aorta. It was seen that based on the site of impact and occupant seating position, the distance/gap from the intruding B-pillar/side door structures and the thorax varied. Further, a comparison of relative motion of the sternum and thoracic spine revealed significant relative motion based on PDOF and seating position (Fig. 7).

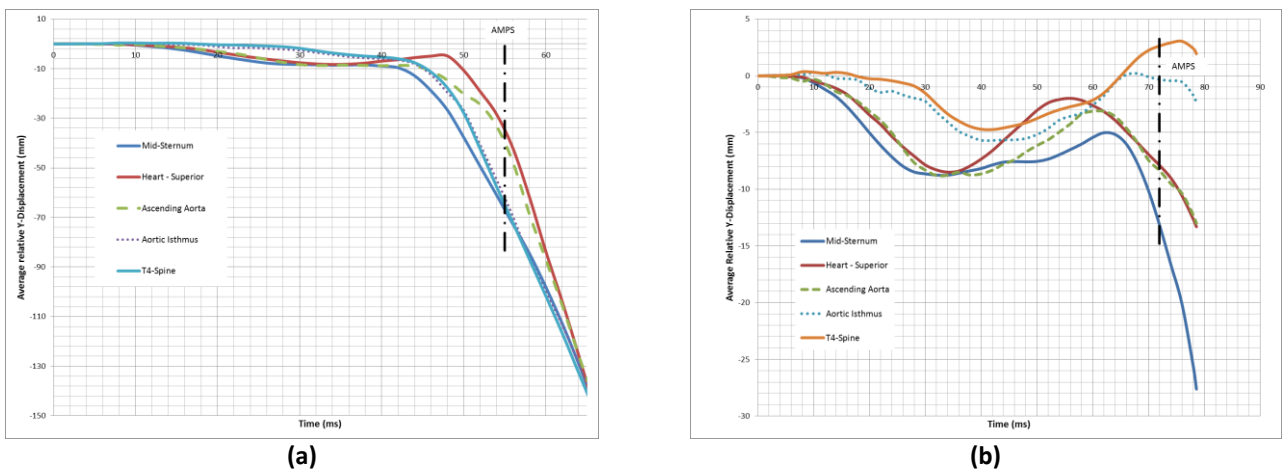


Fig. 7: Relative motion between the spine and sternum (a) PDOF = 260 degrees (b) PDOF = 300 degrees

In order to further delineate the effect of PDOF and to include the role of the other four design factors (Impact position, velocity, occupant position and bumper profile height) on the kinematics on the aortic arch motion, a paired sensitivity analysis was performed by varying only the PDOF within groups. Table 7 lists the configurations for four paired tests selected for simulations as well as model-predicted AMPS and maximum pressure.

Table 7: Paired sensitivity table to access the mechanism of injury based on PDOF

PDOF (Degrees)	Impact Position (mm)	Velocity (km/hr)	Occupant Position (mm)	Bumper Profile Height	Maximum Simulation Time (ms)	AMPS	Time at AMPS (ms)	Maximum Pressure (kPa)	Time at Maximum Pressure (ms)
260	0	54.9	-125	Low	42	0.162	42	127.1	40
270	0	54.9	-125	Low	49	0.281	40	126.3	40
250	0	54.9	0	Low	44	0.258	43	117.7	42
270	0	54.9	0	Low	52	0.324	40	135.1	36
310	0	54.9	125	Low	80	0.054	74	108.5	72
270	0	54.9	125	Low	70	0.152	54	110.8	54
310	0	54.9	0	Low	78	0.067	78	104.4	70
260	0	54.9	0	Low	100	0.204	54	115.2	54

Fig. 8 through Fig. 11 compares and tracks the motion of 18 nodes on the sternum, heart, aortic root, ascending, arch, isthmus and descending aorta along with the thoracic vertebrae for the entire duration of the simulation. In order to compare the kinematics of the aortic arch with the published literature, and to ensure consistency, the exact same nodes were tracked in all the runs.

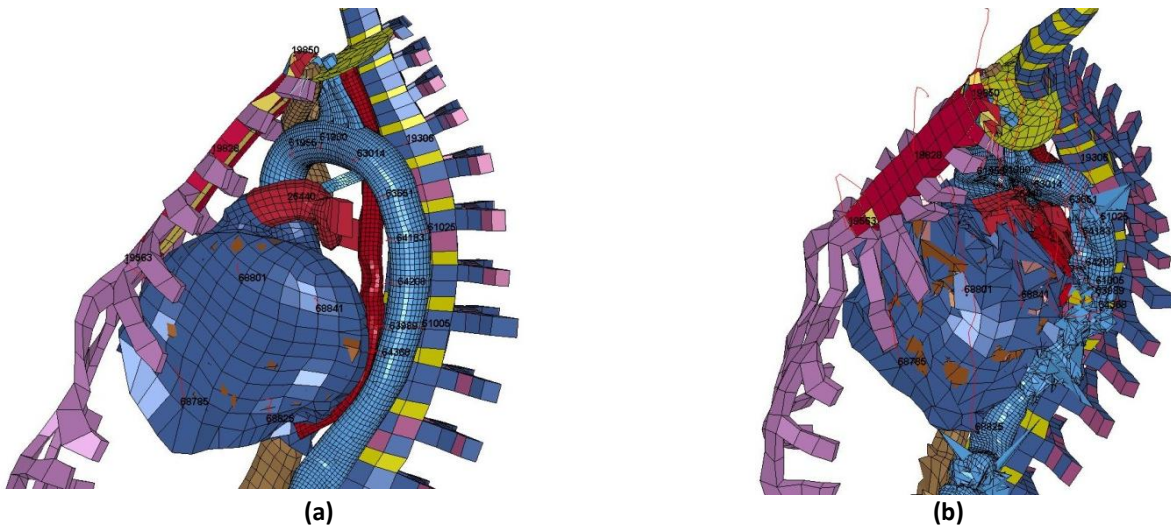


Fig. 8: a) PDOF=260 degrees b) PDOF=270 degrees

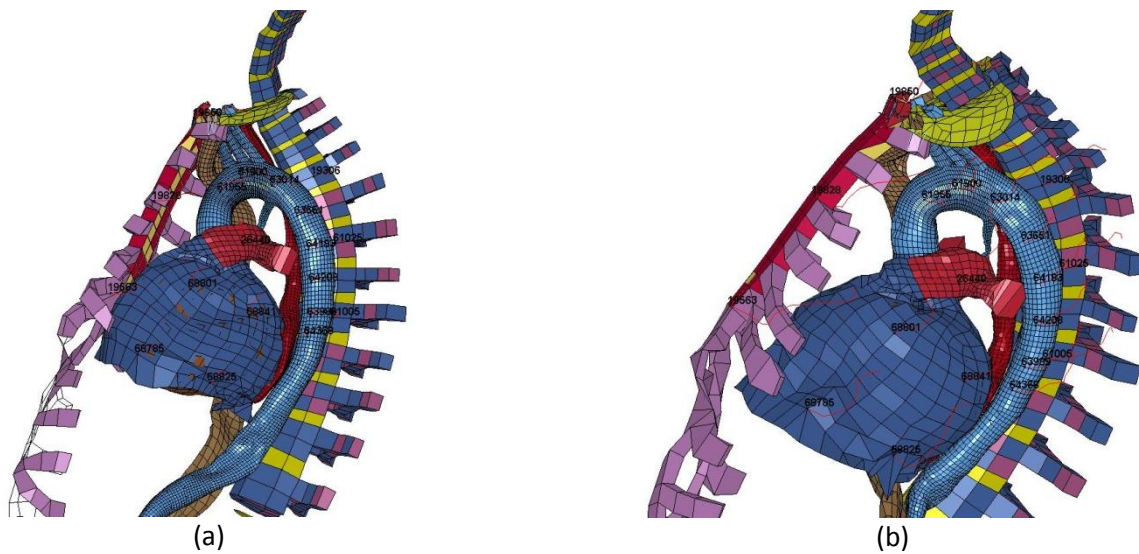


Fig. 9: a) PDOF=250 degrees b) PDOF=270 degrees

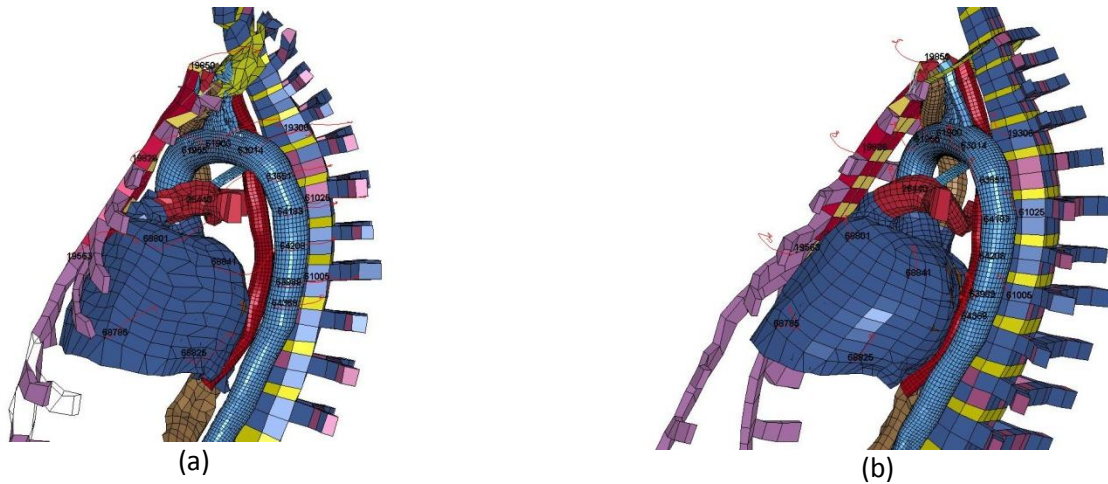


Fig. 10: a) PDOF=310 degrees b) PDOF=270 degrees

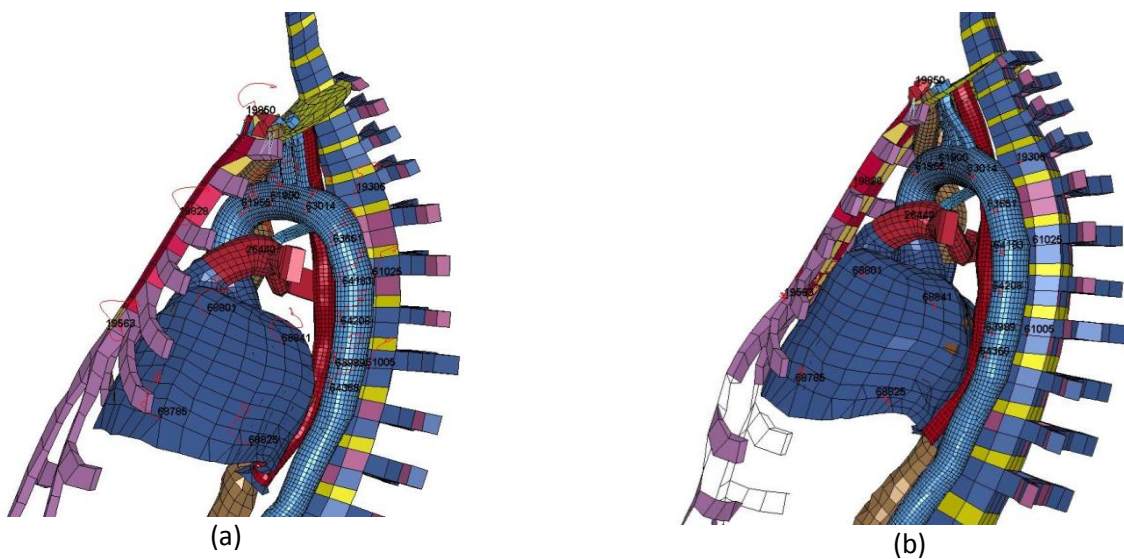


Fig. 11: a) PDOF=310 degrees b) PDOF=260 degrees

It was seen that as the PDOF increased (from 250 degrees), isthmic strain due to longitudinal stretch of the thoracic aorta transitioned from caudomedial motion of the thoracic spine relative to the sternum owing to thoracic deformation from the B-pillar (Fig. 2b) to posterior-anterior motion of the thoracic aorta relative to the ascending aorta (310 degree impact). Kinematics data from the simulations showed that the isthmus of the aorta moved medially and anteriorly during nearside left lateral impacts and transitioned to a dorsocranial motion. This was in concurrence with the kinematics data published by [10] where the motions of the aorta were tracked using high-speed biplanar radiographic method using perfused inverted cadavers.

Several limitations of the current study are noted. Although FE car models were scaled to match, the size and weight of struck and striking vehicles, stiffness, and interior compartment details were not altered. Bumper profiles of the striking vehicle and status of pre-crash braking were different, thus generating varying crush patterns, which may explain the discrepancies in matching the measured physical deformations. Further, measured external deformations may not reflect the dynamic deformations during crashes and may not correspond to compartment intrusions due to differences in elastic moduli of various interior components. The problem is exacerbated from the fact that deformation profiles are measured at only six individual points (SAE J244) on the external surface leading to variations in actual and simulated profiles. It is also to be noted that in the current study only one percentile (50th) of the WSHBM was used for all of the CIREN reconstructions.

V. CONCLUSIONS

The average AMPS recorded in eight nearside left lateral cases was 0.217 ± 0.059 while the average maximum pressure was 117.01 ± 14.67 kPa. For the two victims who sustained a non-fatal aortic injury (Cases #4 and #17),

the average AMPS was 0.169 and the average maximum pressure was 109.3 kPa. On the other hand, for the six cases with a fatal TRA crash, the average AMPS was 0.232 ± 0.057 and the average maximum pressure was 119.58 ± 16.05 kPa. In all of the cases, failure location matched closely with that reported in the autopsy report (CIREN data) and was localized to the isthmus region of the aorta, distal to the left subclavian artery. A 50% risk of aortic failure was 16.5% strain based on AMPS and 97 kPa based on maximum pressure in the aorta. Alternatively, a 90% risk of failure for AMPS was 22% strain and 130 kPa for maximum pressure in the aorta.

From the current CIREN accident injury reconstructions, DOCE and the sensitivity study, we can conclude:

- In all of the cases reconstructed using scaled vehicle models and the WSHBM, aortic strain primarily occurred in the isthmus region of the aorta, distal to the left subclavian artery.
- Average maximum principal strain and maximum pressure in the aorta was in the range of data published by references [1], [9], and [25].
- In nearside pure left lateral impacts (PDOF of 270 degrees), AMPS and maximum pressure was the highest and the isthmus of the aorta moved medially and anteriorly.
- Aortic arch moved dorsocranially due to compression of the anterior chest cavity in cases where the PDOF was greater than 300 degrees.

VI. ACKNOWLEDGEMENT

The authors are grateful to the Southern Consortium for Injury Biomechanics (SCIB) for funding the project. The efforts of Dr. John H. Siegel from the University of Medicine and Dentistry, New Jersey-New Jersey Medical School are greatly appreciated for providing access to the CIREN database. The authors would also like to thank Mr. Suresh Mahi from the Mechanical Engineering department of Wayne State University for his support in analyzing the data. The authors express their gratitude to ESTECO North America for providing modeFRONTIER 4.0. The primary author was supported by the 2009 Drs. Anthony and Kales scholarship.

VII. REFERENCES

- [1] Bass, C.R., Darvish, K., Bush, B., Crandall, J.R., Srinivasan, S.C.M., Tribble, C., Fiser, S., Tourret, L., Evans, J.C., Patrie, J. and Wang, C., 2001, "Material Properties for Modeling Traumatic Aortic Rupture," *Stapp Car Crash Journal*, Vol. 45.
- [2] Ben-Menachem, Y., 1993, "Rupture of the thoracic aorta by broadside impacts in road traffic and other collisions: further angiographic observations and preliminary autopsy findings," *Journal of Trauma* 35(3): 363-367.
- [3] Cammack, K., Rapport, R. L., Paul, J., and Baird, W. C., 1959, "Deceleration injuries of the Thoracic Aorta," *A.M.A Archives of Surgery* 79(2): 244-251.
- [4] Carson, M. W., and Roach, M. R., 1990, "The strength of the aortic media and its role in the propagation of aortic dissection," *Journal of Biomechanics* 22(6): 579-588.
- [5] Crass, J. R., Cohen, A. M., Motta, A. O., Tomashefski, J. F. J., Wiesen, E. J., 1990, "A proposed new mechanism of traumatic aortic rupture: the osseous pinch," *Journal of Radiology* 176(3), pp. 645 - 649.
- [6] Creasy, J. D., Chiles, C., Routh, W.D., Dyer, R.B., 1997, "Overview of Traumatic Injury of the Thoracic Aorta," 17(1), pp. 27 -45.
- [7] Demetriades D, Velmahos GC, Scalea TM, 2008, "Diagnosis and treatment of blunt thoracic aortic injuries: changing perspectives," *Journal of Trauma*, 64, pp.1415–1419.
- [8] Greendyke, R. M., 1966, "Traumatic rupture of the aorta. Special reference to automobile accidents," *Journal of American Medical Association* 195(7): 119-122.
- [9] Hardy, W. N., Shah, C. S., Kopacz, J. M., Yang, K. H., Van Ee, C. A., Morgan, R., Digges, K., 2006, "Study of Potential Mechanisms of Traumatic Rupture of the Aorta Using In Situ Experiments," *Stapp Car Crash Journal* 50, pp. 247-266.
- [10] Hardy, W. N., Shah, C. S., Mason, M. J., Kopacz, J. M., Yang, K. H., King, A. I., Bishop, J. L., Banglmaier, R. F., Bey, M. J., Morgan, R. M., Digges, K. H., 2008, "Mechanisms of traumatic Rupture of the Aorta and Associated Peri-isthmus Motion and Deformation," *Stapp Car Crash Journal*, 52, pp. 233-265.
- [11] Hass, G. M., 1944, "Types of internal injuries of personnel involved in aircraft accidents," *Journal of Aviation Medicine* 15: 77-84.
- [12] Hossack, D. W., 1980, "Rupture of the aorta in road crash victims," *Aust. NZ J. Surg* 50(2): 136-137.

- [13] Klotz, O. and Simpson, W., 1932, "Spontaneous Rupture of the Aorta," American Journal of Medical Science 184: 455-473.
- [14] Lenth RV (1989) Quick and easy analysis of unreplicated factorials, Technometrics 31:469–473.
- [15] Letterer, E. (1924) Beitrage zur entstehung der aortenruptur an typischer stele. Virchows Archiv fur Pathologische Anatomie und Physiologie und fur Klinische Medizin 253: 534-544.
- [16] Lundevall, J., 1964, "The Mechanism of Traumatic Rupture of the Aorta," Acta pathologica et microbiologica Scandinavica, 62, pp. 34-46.
- [17] Marshall, T. K., 1958, "Traumatic dissecting aneurysms," Journal of Clinical Pathology II: 36-38.
- [18] Melvin, J. W., Baron, K. J., Little, W. C. and T.W., G., 1998, "Biomechanical analysis of Indy race car crashes," Proc. 42nd Stapp Car Crash Conference: 247-266.
- [19] Mohan, D., Melvin, J., 1982, "Failure Properties of Passive Human Aortic Tissue I Uniaxial Tension Tests," Journal of Biomechanics, 15(11), pp. 887-902.
- [20] Oppenheim F., 1918, "Gibt eine spontane ruptur der gesunden aorta und wie kommt es zustande?," *Muenchener medizinische wockenschrift*, pp. 1234–1237.
- [21] Rindfleisch, E., 1893, "Zur entstehung and heilung des aneurysma dissecans aortae," Virch. Arch. Path. Anat. 131: 374-378.
- [22] Roberts, V. L., Jackson, F. R. and Berkas, E. M., 1966, "Heart motion due to blunt trauma to the thorax," Proc. 10th Stapp Car Crash Conference: 242-248.
- [23] Roberts, S. B., Chen, P. H., 1970, "Elastostatic analysis of the human thoracic skeleton," Journal of Biomechanics, 3, pp. 527-545.
- [24] Sauaia, A., Moore, F. A., Moore, E. E., Moser, K. S., Brennan, R., Read, R. A., Pons, P. T., 1995, "Epidemiology of trauma deaths: a reassessment," Journal of Trauma, 38(2), pp. 185-193.
- [25] Sevitt, S. (1977) "The mechanisms of traumatic rupture of the thoracic aorta", British Journal of Surgery, 64:166–173.
- [26] Shah, C. S., Hardy, W. N., Mason, M. J., Yang, K. H., Van Ee, C. A., Morgan, R., Digges, K., 2006, "Dynamic Biaxial Tissue Properties of the Human Cadaver Aorta," Stapp Car Crash Journal, 50, pp. 217-246.
- [27] Shah, C. S., Hardy, W. N., Yang, K. H., Van Ee, C. A., Morgan, R. M., Digges, K. H., 2007, "Investigation of the traumatic rupture of the aorta (TRA) by simulating real-world accidents," Proceedings of the 2007 International Research Council on Biomechanics of Injury, Maastricht, The Netherlands, pp. 349-359.
- [28] Shah, C. S., 2007, "Investigation of Traumatic Rupture of the Aorta (TRA) by Obtaining Aorta Material and Failure Properties and Simulation Real-World Aortic Injury Crashes using the Whole-Body Finite (FE) Human Model," Ph. D. Dissertation, Wayne State University.
- [29] Siegel, J. H., Smith, J. A., Siddiqi, S. Q., 2004, "Change in velocity and energy dissipation on impact in motor vehicle crashes as a function of the direction of crash: key factors in the production of thoracic aortic injuries, their pattern of associated injuries and patient survival, A Crash Injury Research Engineering Network (CIREN) study," Journal of Trauma, 57(4), pp. 760-777.
- [30] Siegel, J.H., Belwadi, A., Smith, J.A., Shah, C., Yang, K., 2010, "Analysis of the Mechanism of Lateral Impact Aortic Isthmus Disruption in Real-Life Motor Vehicle Crashes Using a Computer-Based Finite Element Numeric Model: With Simulation of Prevention Strategies," Journal of Trauma, 68, pp. 1375–1395.
- [31] Strassmann, G., 1947, "Traumatic Rupture of the Aorta," American Heart Journal 33: 508-515.
- [32] Taylor, E. R., 1962, "Thrombocytopenia following abrupt deceleration," ARL-TDR-62-30, 6571st ARL, AMD, AFSC, Holloman AFB, New Mexico.
- [33] Vande Geest, J. P., Sacks, M. S. and Vorp, D. A., 2002, "Age-related Differences in the Biaxial Biomechanical Behavior of Human Abdominal Aorta," Proc. of IMECE, 2002 ASME International Mechanical Engineering & Exposition, New Orleans, LA.
- [34] Viano, D., 2011, "Chest Impact Experiments Aimed at Producing Aortic Rupture," Clinical Anatomy
- [35] Voigt, G. E. and Wilfert, K., 1969, "Mechanisms of injuries to unrestrained drivers in head-on collisions," Proceeding 13th Stapp Car Crash Conference: 295-313.
- [36] Zehnder, M. A., 1960, "The mechanism and mechanics of the accident in aortic rupture due to closed thoracic trauma," Thoraxchirurgie, 8, pp. 47-65.